Directional solidification with interface dissipation

A. Classen, C. Misbah,* H. Müller-Krumbhaar, and Y. Saito†
Institut für Festkörperforschung des Forschungszentrums, Jülich, D-5170 Jülich, Germany
(Received 30 October 1990)

The front dynamics during directional solidification of a dilute binary mixture with noninstantaneous interface kinetic attachment is investigated in the weakly and highly nonlinear regimes. In the linear regime we find that, even for small enough kinetic coefficient, the most unstable mode is appreciably modified. With the help of multiscale analysis, we derive the amplitude equation that governs the front dynamics close to criticality. It is found that, for the case of a constant miscibility gap, studied here, the supercritical nature of the bifurcation remains unaltered. However, the computation of the Landau coefficient shows that the interface excursion is reduced by kinetics. Moreover, the analysis of the Mullins-Sekerka spectrum close to the instability threshold indicates that higher harmonics should be activated by interface kinetics. This is confirmed numerically. We study the transition from cells to dendrites by adopting a recent code to the present situation. We find scaling laws that confirm those obtained in the free-growth situation [Brener and Mel'nikov (unpublished)]. The interface structure is "angular," and side branches are much less pronounced, even when the Péclet number exceeds a few unities, than those obtained in the free-kinetics case [Saito, Misbah, and Müller-Krumbhaar, Phys. Rev. Lett. **63**, 2377 (1989)]. Our findings agree well with experiments [P. Kurowski, C. Guthmann, and S. de Cheveigné (unpublished)] on impure CBr_4. We speculate that dendrites in this system are selected by kinetic anisotropy rather than by surface-tension anisotropy.

I. INTRODUCTION

Directional solidification has received an increasing amount of both experimental and theoretical interest[1] during the past few years, not only because of its potential technological importance, but also because it constitutes an interesting nonequilibrium pattern-forming system that continues to reveal a variety of fascinating new phenomena. When a dilute binary solid is grown at the expense of its melt by translating the sample at a constant speed across a temperature gradient, the planar front loses its stability at a critical pulling speed to assume a parallel array of cellular shapes, which upon increasing speed form needlelike structures, before dendrites appear. The first studies of periodic cellular pattern were performed in the weakly nonlinear regime.[2–6] Unfortunately the range of validity of the amplitude expansion in directional solidification—unlike the Rayleigh-Bénard system—is very narrow, the reason being the mixing of two disparate length scales: the destabilizing material diffusion length (which is at least of the order of a few micrometers) and the stabilizing capillary length (of the order of the atomic scale). As a consequence higher harmonics are active even close to threshold, thus causing finite interface fluctuations that escape, in general, the standard lowest-order amplitude expansions.

An important step towards the understanding of pattern formation in directional solidification came from numerical simulations.[7–11] Recently[10] we presented a dynamical numerical code which allows us to explore, in particular, the dendritic regime. Two major results emerged from that work. (i) Crystalline anisotropy is necessary to stabilize the tips of dendrites, as previously found for the free-growth case. (ii) For large enough velocities, such that the Péclet number (defined here as $P=\lambda/l$, where $l=2D/v$, with D the diffusion constant, v the pulling speed, and λ the interface periodicity) approaches unity, dendritic growth with a strong side-branch activity takes place. We find a quantitative agreement with scaling results calculated for the free-growth situation.

Our results agree well with experiments on succinonitrile-acetone mixtures[12] concerning the morphology and the threshold for the appearance of dendrites. In those experiments the dendritic regime is apparent when P is close to unity. However, this is not the case for the CBr_4-Br_2 material.[13,14] Indeed the front exhibits an "angular" structure with no noticeable side branches, even for Péclet numbers of a few units. The question thus arises of whether such a behavior is a signature of a fundamental ingredient that is missing in what is usually called the "minimum version" of crystal growth. One of the most serious points that is emphasized by the derivation of the growth equations is that the chemical boundary condition is an equilibrium condition. This is the so-called limit of diffusion control because all of the reaction rates take place in the diffusion field. It has often been argued in the literature that the interface dissipation can legitimately be neglected provided that the growth velocity is not too large (<1 cm/s). This is likely an overestimation. Of course the absence of a complete microscopic description constitutes a major handicap for a precise estimation on the importance of kinetics. Here we will include the kinetic effect. A result to emerge in this paper is that the overall dendritic shape selected by kinetic anisotropy is similar to that observed on impure CBr_4. Our results, when compared with experiments, give indications on the magnitude of the kinetic

 ©1991 The American Physical Society

coefficient. We will assume a linear law. This means that we assume a rather fast kinetics in a phenomenological picture à la Onsager. All kinds of two-dimensional (2D) nucleation or screw dislocation growth processes are not accounted for in the present work.

The scheme of this paper is as follows. In Sec. II we write down the growth equations. In Sec. III we study the linear stability of the planar front. Section IV deals with the weakly nonlinear regime. By means of multiscale analysis we derive the amplitude equation which governs the interface dynamics close to the instability threshold. We study the nature of the bifurcation and discuss the limit of validity of the amplitude equation. Section V contains discussions of the results in that regime. Section VI is devoted to the highly nonlinear regime. We pay special attention to the dendritic regime. We compare the present results with the previous ones where kinetics were disregarded.[10] Our scaling results are confronted with those obtained in the free-growth situation.[15] Some long formulas have been relegated to the Appendix.

II. BASIC EQUATIONS

We consider the following situation: a dilute binary mixture with a solute concentration C (C is the mass fraction) is pulled in the $(-\hat{\mathbf{z}})$ direction at constant velocity v. The concentration far ahead of the front is fixed at a value C_∞. As usual, we neglect mass diffusion in the solid, since the corresponding diffusion coefficient $D_s \simeq 10^{-11}-10^{-10}$ cm^2/s, while in the liquid $D \sim 10^{-5}$ cm^2/s. The temperature fields in both phases are assumed to be in a steady state and to satisfy Laplace's equation. This assumption is justified by the fact that thermal diffusivities are several orders of magnitude larger than chemical diffusivities so that the temperature fields relax very quickly to their steady-state values. Moreover we assume that heat diffusion takes place symmetrically in both phases and that the latent heat that evolves during solidification plays essentially no role. The first situation can be realized by using highly conducting plates so that the heat diffusion occurs mainly along the plates. Neglecting the latent heat simply means that we assume that it diffuses much faster than the solute produced at the interface. With these assumptions the concentration and temperature fields decouple completely. We are then left with only one field variable, namely, the concentration one, the temperature being fixed by the external thermal contacts. We consider one-dimensional deformations and suppose that the system is quasi-infinite (on the scale of all wavelengths of interest). Let $u=(C-C_\infty)/\Delta C$ denote the dimensionless concentration, $\Delta C=(1-k)C_\infty/k$, where k is the partition coefficient. The equation governing mass transport reads, in the laboratory frame,

$$\nabla^2 u+\frac{2}{l}\frac{\partial u}{\partial z}=\frac{1}{D}\frac{\partial u}{\partial t}\ , \tag{1}$$

where $l=2D/v$ is the diffusion length. At the liquid-solid interface $[z=\zeta(x,t)]$ the mass balance equation takes the form

$$[1+(u-1)(1-k)]v_n=-D\frac{\partial u}{\partial n}\ , \tag{2}$$

where v_n is the normal velocity. Equations (1) and (2) must be supplemented with kinetic equations relating the mass currents of the two species to the chemical potential differences across the interace. We shall only consider situations where the departure from local equilibrium at the interface is small enough for a linear response theory to be valid. We indeed expect a linear law to accurately describe the chemical attachment for a molecularly rough interface. The first step consists in expanding the chemical potentials to first order in the deviation from the pure solvant state, taking the liquid pressure as a reference. Then writing that the chemical potential differences are, in an Onsager picture, proportional to the mass currents across the interface, we obtain the modified Gibbs-Thomson equation

$$u=1-d\kappa-\frac{\zeta}{l_T}+B_{\rm kin}(v-v_n)\ , \tag{3}$$

where $d=\gamma T_m/L|m_l|\Delta C$ is the capillary length, with γ the surface tension, T_m the melting temperature of the pure substance, m_l the liquidus slope, and L the latent heat of fusion per unit volume; $l_T=G|m_l|/\Delta C$ is the thermal length, where G is the applied thermal gradient. $B_{\rm kin}$ denotes a phenomenological kinetic coefficient. In general both d and $B_{\rm kin}$ are orientation-dependent quantities. For a fourfold crystalline anisotropy, considered here, $B_{\rm kin}$ and d read

$$B_{\rm kin}=b_{\rm kin}[1-\alpha_{4\,\rm kin}\cos(4\theta)]\ , \tag{4a}$$

$$d=d_0[1-\alpha_4\cos(4\theta)]\ , \tag{4b}$$

where θ is the angle between the normal to the interface and the z axis, $b_{\rm kin}$ and d_0 are constant factors, and the α's represent the strength of the crystalline anisotropy (we assume that the α's account for both the force and torque contributions). Note that in Eq. (3) we have taken the origin of the z axis such that the planar front sets at $z=0$ instead of $z=-B_{\rm kin}l_T v_0$, which corresponds to the amount of the planar front recession due to kinetics. Equations (1)–(4) with the boundary condition $u(z=\infty)=0$ completely describe the motion of the solidification front. These equations admit a planar front solution characterized by $\zeta=0$ and $u\equiv u_0(z)=e^{-2z/l}$.

III. LINEAR STABILITY ANALYSIS

We study the regression of small interface fluctuations by considering solutions of the form

$$\zeta=\epsilon\zeta_{11}e^{iqx+\omega t}\ , \tag{5a}$$

$$u=u_0(z)+\epsilon u_{11}(z)e^{iqx+\omega t}\ , \tag{5b}$$

where ϵ is a small parameter, q the wave number of the perturbation, and ω is the amplification (or attenuation) rate that we wish to determine. Note that since we are interested in this section with the linear analysis, we only need to consider one Fourier component. We do not take crystalline anisotropy into account in this section. Insert-

ing Eq. (5b) into Eq. (1) we obtain by solving the resulting equation and imposing $u_{11}(z=\infty)=0$,

$$u_{11}(z)=\beta_{11}e^{-mz}, \tag{6}$$

with $m=1/l+(q^2+1/l^2+\omega/D)^{1/2}$ and where we have required that $\mathrm{Re}(m)>0$. β_{11} is an integration constant. Evaluating Eqs. (2) and (3) to first order ϵ and using Eqs. (5) and (6) we obtain

$$v(1-k)\left[\frac{\beta_{11}}{\zeta_{11}}-\frac{2}{l}\right]+\omega=-\frac{2v}{l}+\frac{mD\beta_{11}}{\zeta_{11}}, \tag{7a}$$

$$\frac{\beta_{11}}{\zeta_{11}}=-\left[d_0q^2+\frac{1}{l_T}+b_{\mathrm{kin}}\omega\right]k. \tag{7b}$$

The compatability condition that emerges from the above linear set of algebraic equations results in the dispersion relation sought:

$$\omega=v\frac{(k-1+ml/2)(-d_0q^2-1/l_T+2/l)-2k/l}{1+vb_{\mathrm{kin}}(ml/2+k-1)}. \tag{8}$$

In the absence of kinetics, $b_{\mathrm{kin}}=0$, we recover the Mullins-Sekerka[16] dispersion relation, which has been extended to non-quasi-steady growth by Wollkind and Segel.[2] The growth rate given by Eq. (8) may *a priori* be complex, at least in a certain domain of wave numbers. Since we are interested in the onset of the planar front instability, we simply need to study Eq. (8) close to the neutral point(s). We show here that, as in the free-kinetics situation,[2] the stability exchange principle is satisfied. For this purpose let us set

$$\omega=\mathrm{Re}(\omega)+i\,\mathrm{Im}(\omega)\equiv\omega_r+i\omega_i.$$

Substituting ω into Eq. (8) and assuming $\omega_r=0$, we find

$$v\left[(2l^{-1}-d_0q^2-l_T^{-1})\left\{k-\tfrac{1}{2}+\frac{1}{2\sqrt{2}}\left[\left[1+q^2l^2+\frac{\omega_I^2l^4}{D^2}\right]^{1/2}+1+q^2l^2\right]^{1/2}\right\}-\frac{2k}{l}\right]$$
$$+\frac{2b_{\mathrm{kin}}\omega_I^2l}{\sqrt{2}[(1+q^2l^2+\omega^2l^4/D^2)^{1/2}+1+q^2l^2]^{1/2}}=0 \tag{9a}$$

and

$$\omega_I\left[1-\frac{1-l/2l_T-d_0lq^2/2}{(1/\sqrt{2})[(1+q^2l^2+\omega_I^2l^4/D^2)^{1/2}+1+q^2l^2]^{1/2}}\right.$$
$$\left.+vb_{\mathrm{kin}}\left\{k-\tfrac{1}{2}+\frac{1}{2\sqrt{2}}\left[\left[1+q^2l^2+\frac{\omega_I^2l^4}{D^2}\right]^{1/2}+1+q^2l^2\right]^{1/2}\right\}\right]=0. \tag{9b}$$

Since

$$\left[\left[1+q^2l^2+\frac{\omega_I^2l^4}{D^2}\right]^{1/2}+1+q^2l^2\right]^{1/2}>\sqrt{2}$$

the second term in the bold parentheses in Eq. (9b) is always smaller than 1 and the third term ($\sim b_{\mathrm{kin}}$) is always positive. In other words, the factor multiplying ω_I in Eq. (9b) is always positive, which entails that the only solution to Eq. (9b) is the trivial one, namely, $\omega_I=0$. This means that the bifurcation from the planar solution to the deformed one is steady, and when looking for the instability threshold we can simply set $\omega=0$ in Eq. (8).

The surface of bifurcation in the parameter space is determined by the parametric equations

$$\omega=0 \quad \text{and} \quad \frac{\partial\omega}{\partial q}=0. \tag{10}$$

Using Eq. (8) we obtain at the bifurcation

$$\left[\frac{ml}{2}-1+k\right]\left[\frac{2}{l}-d_0q^2-\frac{1}{l_T}\right]-\frac{2k}{l}=0, \tag{11a}$$

$$\frac{d_0}{l}=\frac{k}{2(ml-1)(ml/2+k-1)^2}. \tag{11b}$$

Equations (11a) and (11b) determine, for a given thermal length l_T, the critical wave number q_c and the critical velocity (or diffusion length) v_c for the onset of the Mullins-Sekerka[16] instability. Note that Eqs. (11a) and (11b) are kinetics independent, thus indicating that the location of the bifurcation is not affected by kinetics. Therefore the analysis of the bifurcation point is exactly the one done by Mullins-Sekerka[16] (see also Ref. 2).

IV. THE WEAKLY NONLINEAR REGIME

The linear stability analysis is the first step in any stability problem. Moreover it is a natural starting point for the definition of the nonlinear problem. In this section we are interested in the front dynamics in the weakly nonlinear regime. This means that we concentrate on the situation near the bifurcation point. This will allow us to extract from the full growth equations the only part that is relevant to the dynamics close to criticality. To deal with this question we will make use of a multiscale analysis analogous to that performed by Newell, Whitehead,[17] and Segel[18] in the context of the Rayleigh-Bénard problem. To do so we must first specify the characteristic time and space scales. Equations (11a) and (11b) deter-

mine the critical conditions for the onset of the Mullins-Sekerka[16] instability and the wave number q_c of the bifurcating state. Let v_c denote the critical velocity at a given thermal gradient (i.e., a given thermal length). If v is increased slightly above v_c, the growth rate ω as a function of q has the shape sketched in Fig. 1. As shown in this figure there is a band Δq of wave numbers which corresponds to exponentially growing modes. This means that the linear approximation will cease to be valid and we should no longer ignore nonlinear effects. Close to the threshold $\omega(v,q)$ given by Eq. (8), can be written to leading order as

$$\omega(v,q)\simeq(v-v_c)\frac{\partial\omega}{\partial v}+\tfrac{1}{2}(q-q_c)^2\frac{\partial^2\omega}{\partial q^2}\ , \tag{12}$$

where derivatives are understood to be evaluated at the critical point (q_c,v_c). If $v-v_c$ is of order ϵ^2, this means that the band of active modes that can be used to construct the wave packet is $\Delta q\sim O(\epsilon)$. This implies that the characteristic length Δx for the modulation of the wave packet in real space is of order $\Delta x\sim 1/\Delta q\sim\epsilon^{-1}$. The strategy of the multiscale analysis is to separate the fast interface modulation, whose dynamics is dominated by the critical mode ($\sim e^{iq_c x}$), from these slow ones that characterize the large-scale distortion of the pattern. We then introduce a slow variable $X=\epsilon x$. On the other hand, because $\omega\sim O(\epsilon^2)$ [since $(v-v_c)\sim\epsilon^2$], we may expect that the characteristic time scale for the motion of interest is of order ϵ^{-2}. Accordingly we introduce a slow time $\tau=\epsilon^2 t$. We then write each quantity (e.g., u,ζ) formally as if it depended separately on (x,X,τ). Therefore we are to understand that we should make the substitutions

$$\frac{\partial}{\partial x}\to\frac{\partial}{\partial x}+\epsilon\frac{\partial}{\partial X}\ , \tag{13a}$$

$$\frac{\partial}{\partial t}\to\epsilon^2\frac{\partial}{\partial\tau} \tag{13b}$$

whenever we differentiate u and ζ. The last step consists of expanding u and ζ in power series of ϵ around the planar front solution

$$u=u_0(z)+\epsilon u_1(x,X,z,\tau)+\cdots\ , \tag{14a}$$

$$\zeta=0+\epsilon\zeta_1(x,X,\tau)+\cdots\ . \tag{14b}$$

Now the scheme is to insert Eqs. (13) together with (14) into the basic equations (1)–(3) and use the resulting equations to deduce successively higher-order contributions in an expansion in powers of ϵ. The small parameter ϵ is defined as the square root of the growth rate, resulting from the linear analysis, evaluated at the critical wave number and at the actual velocity ($v\geq v_c$), $\epsilon=[\omega(q_c,v)]^{1/2}$. It then follows from Eq. (12) that

$$\epsilon^2=(v-v_c)\left[\frac{\partial\omega}{\partial v}\right]_{q=q_c} \tag{15}$$

which constitutes the appropriate small parameter [instead of $(v-v_c)/v_c$; see below].

(i) Order ϵ. By using Eqs. (13) and (14), Eq. (1) provides to this order

$$L_0u_1\equiv\left[\frac{\partial^2}{\partial x^2}+\frac{\partial^2}{\partial z^2}+\frac{2}{l}\frac{\partial}{\partial z}\right]u_1=0\ . \tag{16}$$

This equation is solved by

$$u_1=\tfrac{1}{2}A(X,\tau)e^{iq_c x}u_{11}(z)+\text{c.c.}\ , \tag{17}$$

where

$$u_{11}(z)=\beta_{11}e^{-m_c z} \tag{18}$$

with

$$m_c=\frac{1}{l}+\left[\frac{1}{l^2}+q_c^2\right]^{1/2}\ . \tag{19}$$

β_{11} is a real constant and $A(X,\tau)$ is a complex amplitude, which is an integration factor depending on the slow variables X,τ. This amplitude is unknown at this order. In Eq. (17) we have deliberately, in a multiscale spirit, separated the fast variation $e^{iq_c x}$ from the slow modulations absorbed in the complex amplitude $A(X,\tau)$. Note that expression (17), where u_{11} is given by Eq. (18), is nothing but the linear deviation about the planar front solution expressed by the second term on the right-hand side of Eq. (5b) in which we set $q=q_c$. The difference between that expression and the one given in Eq. (17) is that here the prefactor A is a space- and time-dependent quantity, which will be determined at order ϵ^3. The dependence on X and τ expresses the fact that the interface dynamics are not only governed by the critical mode $e^{iq_c x}$ but also by the active modes with wave numbers lying inside the linearly unstable band Δq (see Fig. 1).

At this order, the interface fluctuation can be written as

$$\zeta_1=\tfrac{1}{2}\zeta_{11}A(X,\tau)e^{iq_c x}+\text{c.c.}\ , \tag{20}$$

where ζ_{11} is a constant factor. Inserting this expression into the Gibbs-Thomson condition (3), using Eq. (17), and collecting the terms proportional to ϵ we obtain

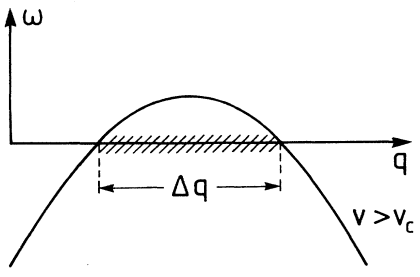

FIG. 1. Schematic plot of the dispersion relation above the Mullins-Sekerka threshold. Δq designates the band of unstable modes.

$$\beta_{11}/\zeta_{11}=\frac{2}{l}-\frac{1}{l_T}-d_0q_c^2 \ . \tag{21}$$

Imposing mass conservation [Eq. (2)] we obtain another expression for this ratio. Equating the two expressions we obtain a solvability condition which is simply the dispersion relation (8) evaluated at the critical point.

(ii) Order ϵ^2. To this order, and after making use of the results obtained in the previous order, the bulk equation (1) reads

$$L_0u_2=-2u_{11}\,\mathrm{Re}\left[iq_ce^{iq_cx}\frac{\partial}{\partial X}A\right] \ . \tag{22}$$

The interface equation (2) takes the form

$$\frac{2v_ck\zeta_2}{l}+D\frac{\partial}{\partial z}u_2+v_c(1-k)u_2=\left[\frac{kv_c}{l^2}+\frac{k/l}{lm_c/2+k-1}(-2Dm_c^2+2v_cm_c-v_ckm_c)\right]\mathrm{Re}(A^2e^{2iq_cx})$$
$$+\left[\frac{kv_c}{l^2}-v_ckm_c\frac{k/l}{lq_c/2+k-1}\right]\|A\|^2 \tag{23}$$

while the Gibbs-Thomson condition (3) provides

$$u_2+\frac{2\zeta_2}{l}+d_0\frac{\partial^2}{\partial x^2}\zeta_2-\frac{\zeta_2}{l_T}=\left[\frac{1}{l^2}-\frac{m_ck/l}{lm_c/2+k-1}\right][\mathrm{Re}(A^2e^{2iq_cx})+\|A\|^2]$$
$$-2d_0\,\mathrm{Re}\left[iq_ce^{iq_cx}\frac{\partial}{\partial X}A\right]+\tfrac{1}{4}b_{\mathrm{kin}}v_cq_c^2[\mathrm{Re}(A^2e^{2iq_cx})-\|A\|^2] \ . \tag{24}$$

The right-hand sides of Eqs. (22)–(24) contain the inhomogeneous part. There appear three types of terms, which are proportional to $\|A\|^2$, $e^{iq_cx}(\partial/\partial X)A$, and $A^2e^{2iq_cx}$. This structure suggests that one should seek the second-order contribution in the following form:

$$\zeta_2=\zeta_{20}\|A\|^2+\zeta_{21}\,\mathrm{Re}\left[ie^{iq_cx}\frac{\partial}{\partial X}A\right]$$
$$+\zeta_{22}\,\mathrm{Re}(A^2e^{2iq_cx}) \ , \tag{25a}$$
$$u_2=u_{20}(z)\|A\|^2+u_{21}(z)\mathrm{Re}\left[ie^{iq_cx}\frac{\partial}{\partial X}A\right]$$
$$+u_{22}(z)\mathrm{Re}(A^2e^{2iq_cx}) \ . \tag{25b}$$

Inserting these expressions into Eqs. (22)–(24) and equating the coefficients of 1, e^{iq_cx}, and e^{2iq_cx} on both sides, we obtain inhomogeneous equations for the unknowns ζ_{ij} and $u_{ij}(z)$. The bulk equation (22) gives rise to the following equations:

$$\left[\frac{\partial^2}{\partial z^2}+\frac{2}{l}\frac{\partial}{\partial z}\right]u_{20}=0 \ , \tag{26a}$$
$$\left[\frac{\partial^2}{\partial z^2}+\frac{2}{l}\frac{\partial}{\partial z}-4q_c^2\right]u_{22}=0 \ , \tag{26b}$$
$$\left[\frac{\partial^2}{\partial z^2}+\frac{2}{l}\frac{\partial}{\partial z}-q_c^2\right]u_{21}=-2u_{11}(z)q_c \ . \tag{26c}$$

These equations are solved by

$$u_{20}=\beta_{20}e^{-2z/l} \ , \tag{27a}$$
$$u_{22}=\beta_{22}e^{-m_c'z} \ , \tag{27b}$$
$$u_{21}=\beta_{21}e^{-m_cz}-\frac{\beta_{11}q_c}{1/l-q_c}ze^{-m_cz} \tag{27c}$$

where m_c' is defined in the same ways as m_c from Eq. (19) in which q_c should be replaced by $2q_c$ and β_{ij} are integration factors undetermined for the moment. Inserting (26a)–(26c) into the boundary conditions (23) and (24) we obtain six equations for the coefficients ζ_{ij},β_{ij}. These equations split into three independent sets of algebraic equations for (ζ_{20},β_{20}), (ζ_{22},β_{22}), (ζ_{21},β_{21}). the solution of the first two sets is listed in the Appendix. In contrast to these two sets, the set of equations for (ζ_{21},β_{21}) is singular in the sense that its determinant vanishes. To see this we simply need to realize that ζ_{21} and β_{21} (via u_{21}) multiply the fundamental harmonic in Eq. (25), exactly as do β_{11} and ζ_{11} in the linear stability problem [Eqs. (5a) and (5b)]. We know from this problem that the determinant of the associated set of equations [Eqs. (7a) and (7b)] precisely vanishes at the bifurcation. The difference here is that the set of equations for (ζ_{21},β_{21}) is inhomogeneous, as signaled by the presence on the right-hand sides of Eqs. (22)–(24) of the fundamental harmonic. Therefore to make this system solvable we should impose a solvability condition, which, after some simple algebraic manipulations, takes the form

$$\frac{d_0}{l}=\frac{k}{2(m_cl-1)(lm_c/2+k-1)^2} \ . \tag{28}$$

This expression is exactly the one given by Eq. (11b) eval-

uated at the bifurcation. We should point out that the two solvability conditions obtained at the previous and at this order are nothing but the bifurcation equations [Eq. (10)]. In other words, the present solvability condition does not contain additional information. The really interesting result appears in the next order. The solvability condition becomes a constraint for $A(X,\tau)$ which constitutes the amplitude equation we wish to determine

(iii) Order ϵ^3. Expanding the basic equations (1)–(3) up to third order and using the results obtained at previous orders we find that the bulk equations satisfy

$$L_0 u_3 = \frac{u_{11}}{D}\mathrm{Re}\left[e^{iq_c x}\frac{\partial}{\partial\tau}A\right] - u_{11}\,\mathrm{Re}\left[e^{iq_c z}\frac{\partial^2}{\partial X^2}A\right] + 2q_c u_{21}\,\mathrm{Re}\left[e^{iq_c x}\frac{\partial^2}{\partial X^2}A\right] - 8q_c u_{22}\,\mathrm{Re}\left[ie^{2iq_c x}A\frac{\partial}{\partial X}A\right] \tag{29}$$

and the Gibbs-Thomson condition (3) becomes

$$u_3 + \left[\frac{1}{l_T}-\frac{2}{l}\right]\zeta_3 - d_0\frac{\partial^2}{\partial x^2}\zeta_3 = \left\{\left[-\frac{4\zeta_{20}}{l^2}+\left[\frac{m_c\beta_{11}}{2}-\frac{2}{l^2}+b_{\mathrm{kin}}v_c q_c^2\right]\zeta_{22}+\frac{2\beta_{20}}{l}+\frac{m_c'\beta_{22}}{2}+\frac{1}{l^3} - \tfrac{3}{8}m_c^2\beta_{11}+\tfrac{3}{8}d_0 q_c^4\right]\|A\|^2+\alpha+d_0(1-2q_c\zeta_{21})\frac{\partial^2}{\partial X^2}-b_{\mathrm{kin}}\frac{\partial}{\partial\tau}\right\}\mathrm{Re}(Ae^{iq_c x})+\cdots, \tag{30}$$

where the ellipsis represents other harmonics and $\alpha=[(\partial/\partial\omega)(2/l-1/l_T)]_{\omega=0}$. Its explicit form is listed in the Appendix. Note that we have omitted in Eq. (30) the other harmonics since they are not "secular" in the sense that they do not break the uniformity of the ϵ expansion. Stated in another way, the other harmonics are not resonant and therefore do not give rise to any nontrivial solvability condition.

Finally the third-order contribution to the continuity equation (2) can be written as

$$\frac{2}{l}k\zeta_3+\frac{l}{2}\frac{\partial}{\partial z}u_3+(1-k)u_3 = \left[\left[\frac{4}{l^2}k-\frac{l}{2}m_c^2\beta_{11}+(1-k)m_c\beta_{11}\right]\zeta_{20} + \left[\frac{2}{l^2}k+\frac{l}{2}q_c^2-\frac{l}{4}m_c^2\beta_{11}+(1-k)m_c\beta_{11}\right]\zeta_{22}+\frac{k}{l^3}+\tfrac{3}{16}lm_c^3\beta_{11} - \frac{l}{8}m_c q_c^2\beta_{11}-\tfrac{3}{8}(1-k)m_c^2\beta_{11}-\frac{2k}{l}\beta_{20}+\left[\frac{l}{2}q_c^2-\frac{l}{4}m_c'^2+\frac{(1-k)m_c'}{2}\right]\beta_{22}\right] \times\|A\|^2\mathrm{Re}(Ae^{iq_c x})-\frac{1}{v_c}\frac{\partial}{\partial\tau}\mathrm{Re}(Ae^{iq_c})+\cdots, \tag{31}$$

where the ellipsis represents other harmonics. The general form of the solution of the third-order problem is

$$\zeta_3=\mathrm{Re}(i\zeta_{31}e^{iq_c x})+\cdots \tag{32a}$$

$$u_3=\mathrm{Re}[iu_{31}(z)F(X,\tau)e^{iq_c x}]+\cdots \tag{32b}$$

where the ellipses represent other harmonics and F is a function of the slow variables, unknown at this order. We have disregarded the other harmonics for the reasons we mentioned above. Inserting (32) into (29)–(31) and equating the coefficients of $e^{iq_c x}$ on both sides we obtain inhomogeneous equations for u_{31} and ζ_{31}. The bulk equation (29) produces

$$\left[\frac{\partial^2}{\partial z^2}+\frac{2}{l}\frac{\partial}{\partial z}-q_c^2\right]\mathrm{Re}(Fu_{31}) = \mathrm{Re}\left\{\left[u_{11}\left[\frac{1}{D}\frac{\partial}{\partial\tau}-\frac{\partial^2}{\partial X^2}\right]+2q_c u_{21}\frac{\partial^2}{\partial X^2}\right]A\right\} \tag{33}$$

whose solution consists of a sum of a homogeneous and a particular solution

$$u_{31}=\beta_{31}e^{-m_c z}+\frac{ze^{-m_c z}}{2F(1/l-q_c)}\times\left[\beta_{11}\left[\frac{1}{D}\frac{\partial}{\partial\tau}-\frac{\partial^2}{\partial X^2}\right]A+\left[2q_c\beta_{21}+\frac{\beta_{11}q_c^2}{(1/l-q_c)^2}\right]\times\frac{\partial^2}{\partial X^2}A\right]. \tag{34}$$

β_{31} is an integration constant. Since u_{31} and ζ_{31} multiply the fundamental harmonic [Eqs. (32a) and (32b)] the associated boundary conditions [Eqs. (30) and (31)] will produce a system of algebraic equations for the unknowns $(F\beta_{31},\zeta_{31})$ whose determinant vanishes rigorously at the

bifurcation. This situation was met in the previous order when we dealt with the system relative to the coefficients (β_{21},ζ_{21}). We should therefore, as discussed before, impose a solvability condition which results here in the complex amplitude equation of the Landau-Ginzburg type,

$$\frac{\partial}{\partial \bar{t}}\bar{A}=\bar{A}-2\bar{q}_c\frac{\partial^2\bar{\omega}}{\partial(\bar{q}^2)^2}\frac{\partial^2}{\partial\bar{X}^2}\bar{A}-\omega_1\|\bar{A}\|^2\bar{A}\ . \tag{35}$$

This equation is written in a dimensionless form, where length and time are reduced by l and l^2/D, respectively. We have expressed the coefficient of $\partial^2\bar{A}/\partial X^2$ as a function of the growth rate $\bar{\omega}$. This coefficient is evaluated at the bifurcation; it is positive since it measures the curvature of the growth rate at the bifurcation point. This is a general result which is met in any stability problem where an initially translationally invariant solution (the planar front in the present case) undergoes a bifurcation at a finite wave number. The Landau coefficient ω_1, whose expression is listed in the appendix may be positive or negative. We will discuss the nature (subcritical or supercritical) of the bifurcation, which is determined by the sign of ω_1, in the next section.

V. DISCUSSIONS OF THE RESULTS IN THE LINEAR AND WEAKLY NONLINEAR REGIMES

In this section we would like to discuss the effect of kinetics in the linear and weakly nonlinear regimes. We have seen from Eqs. (11a) and (11b) that the location of the bifurcation point in the parameter space and the wave number q_c of the bifurcatiing state are not altered by the kinetic effect. Equation (11b) can be rewritten as follows:

$$\bar{d}_0=\frac{k}{2(1+\bar{q}_c^2)^{1/2}[k-\frac{1}{2}+(1/4+\bar{q}_c^2/4)^{1/2}]^2}\ , \tag{36}$$

where

$$\bar{d}_0=\frac{d_0}{l},\quad \bar{q}_c=q_c l \tag{37}$$

are the dimensionless capillary length and the dimensionless critical wave number, respectively. In standard experiments the growth velocity $V\sim 1-100\mu$m/s. The diffusion constant $D\sim 10^{-5}$ cm^2/s. This amounts to $l\sim 10^2-10^5$ μm, while the capillary length is typically $d_0\sim 10^{-2}$ μm. This implies that in general $\bar{d}_0\equiv d_0/l\ll 1$. We then obtain from Eq. (36) that $\bar{q}_c\gg 1$. Equation (36) provides to leading order

$$\bar{q}_c=\left[\frac{2k}{\bar{d}_0}\right]^{1/3} \tag{38}$$

which relates the bifurcation wave number to the reduced capillary length (which is proportional to the growth velocity). The second parametric equation (11b) yields in this regime ($\bar{d}_0\ll 1$; small v)

$$\frac{l_T}{l}\equiv\bar{l}_T=\tfrac{1}{2}\ , \tag{39}$$

which is the well-known constitutional supercooling criterion. Equations (38) and (39) define the critical wave number and the condition for the onset of instability in the small velocity regime. As stated above, these expressions are kinetics independent. However, above the bifurcation we expect the front dynamics to be altered by kinetics. Slightly above the bifurcation ($\bar{l}_T=\frac{1}{2}+\nu$, ν being a small positive parameter) there is a band Δq (see Fig. 1) which corresponds to active modes. The fastest growing mode (which is likely the most active one, at least close to the threshold) corresponds to the maximum growth rate. Since $\bar{q}_c\gg 1$ in the regime of interest, we can rewrite expression (8) to leading order as

$$\bar{\omega}=\frac{\bar{q}(2-1/\bar{l}_T-\bar{d}_0\bar{q}^2)}{1+\bar{q}\bar{b}_{\rm kin}/2}\ , \tag{40}$$

where $\bar{\omega}=\omega l^2/D$ and $\bar{b}_{\rm kin}=2Db_{\rm kin}/l$ are dimensionless quantities. At the fastest rate ($\partial\bar{\omega}/\partial\bar{q}=0$) we obtain from Eq. (40)

$$2-\bar{l}_T^{-1}-3\bar{d}_0\bar{q}^{\,2}-\bar{d}_0\bar{b}_{\rm kin}\bar{q}^{\,3}=0\ . \tag{41}$$

In the absence of kinetics ($\bar{b}_{\rm kin}=0$), the wave number $\bar{q}_{\rm max}$ of the fastest growing mode is given by

$$\bar{q}_{\rm max}=\left[\frac{2-\bar{l}_T^{-1}}{3\bar{d}_0}\right]^{1/2}\ . \tag{42}$$

Note that above the bifurcation $\bar{l}_T^{-1}>2$. In the presence of kinetics Eq. (41) can be solved exactly. We prefer, however, to avoid heavy formulas, to solve this equation perturbatively, by assuming a small $\bar{b}_{\rm kin}$. We should observe that $\bar{b}_{\rm kin}$ plays the role of a singular perturbation in Eq. (41) since it multiplies the term with the highest power ($\bar{q}^3$). It is easy to show that the singular solution is given to leading order by $-3/\bar{b}_{\rm kin}$, which is negative. The solution of interest is the regular one, where $\bar{q}_{\rm max}$ is shifted linearly by kinetics. The shifted solution is easily found to be

$$\bar{q}'_{\rm max}=\bar{q}_{\rm max}\left[1-\frac{\bar{b}_{\rm kin}\bar{q}_{\rm max}}{6}\right]+O_2(\bar{b}_{\rm kin})\ . \tag{43}$$

The effect of kinetics has a tendency to reduce the wave number of the fastest growing mode. We see from Eq. (43) that the condition under which the kinetic effect can be considered as perturbative is that

$$\bar{b}_{\rm kin}\ll\frac{1}{\bar{q}_{\rm max}}\ . \tag{44}$$

If the distance from threshold is small, say, for example, $\bar{l}_T=\frac{1}{2}+0.05$, and if we choose a typical value for the capillary length, $\bar{d}_0=10^{-4}$, we obtain

$$\bar{q}_{c\,\rm max}\sim 10\ . \tag{45}$$

This implies according to Eq. (44) that the effect of kinetics can be treated perturbatively only if $\bar{b}_{\rm kin}$ is restricted to

$$\bar{b}_{\rm kin}\ll 0.1\ . \tag{46}$$

The reason for the importance of kinetic effect, albeit when $\bar{b}_{\rm kin}$ is as small as 0.1, can be understood by noticing that $\bar{b}_{\rm kin}$ multiplies $\bar{q}_c$ in Eq. (8) which is larger compared to unity. The reason that $\bar{q}_c$ is large is that in directional solidification the two competing lengths (the diffusion length and capillary length) have completely different orders of magnitudes. As a consequence, the growth rate of the linearly most unstable mode is significantly reduced by kinetics. On the other hand, because the neutral modes ($\bar{\omega}=0$) are not affected by kinetics, Eq. (46) implies necessarily that the curvature of the Mullins-Sekerka[16] spectrum in the presence of kinetics is smaller than that for the kinetics free case

$$\left[\frac{\partial^2\bar{\omega}}{\partial\bar{q}^2}\right]_{\bar{q}=\bar{q}_{\max},\bar{b}_{\rm kin}\neq 0} < \left[\frac{\partial^2\bar{\omega}}{\partial\bar{q}^2}\right]_{\bar{q}=\bar{q}_{\max},\bar{b}_{\rm kin}=0} . \tag{47}$$

In other words, kinetics makes $\bar{\omega}$ flatter close to threshold. As a result higher harmonics should be activated. We will see in the next section that this is confirmed by our simulation.

Another result found here is that kinetics do not alter the nature of the bifurcation in the case of a constant miscibility gap we are interested in here, for reasons that will become clear later. Specifically, in standard experiments where $\bar{q}_c \gg 1$, an expansion of the Landau constant ω_1 (listed in the Appendix) shows that the leading order ($\bar{d}_0 \ll 1$) reads

$$\omega_1=\frac{1}{16}\left[\frac{2k}{\bar{d}_0}\right]^{2/3}\left[\frac{k^2+4k-2}{4k}\right] + \bar{b}_{\rm kin}\left[\frac{2k}{\bar{d}_0}\right]^{5/3}+\cdots . \tag{48}$$

For $\bar{b}_{\rm kin}=0$ we recover the expression derived by Wollkind and Segel,[2] which indicates, as pointed out by Caroli, Caroli, and Roulet,[5] that the bifurcation is supercritical when $k>0.4$. As the factor multiplying $\bar{b}_{\rm kin}$ is positive, and if the bifurcation is supercritical in the absence of kinetics, its nature remains unchanged. In particular for $k=1$ the bifurcation remains normal. We should note that the term multiplying $\bar{b}_{\rm kin}$ in Eq. (48) is much more dominant than the one obtained in the free-kinetics case, unless $\bar{b}_{\rm kin}$ is extremely small ($\bar{b}_{\rm kin}<10^{-3}$). If we are interested in the situation with $k=1$ then kinetics simply cause the Landau constant to be appreciably larger (for $\bar{b}_{\rm kin}\simeq 0.1$). By computing the full Landau coefficient for $k=1$ we have found that a kinetic coefficient $\bar{b}_{\rm kin}\simeq 0.1$ induces an increase of ω_1 by a factor of about 2. The interface amplitude is $\bar{A}\sim(\bar{\omega}/\omega_1)^{1/2}$. On the other hand, $\bar{\omega}$ decreases with kinetics [Eq. (47)], while ω_1 increases. These two facts induce a reduction of the interface amplitude of the bifurcating state. In other words kinetics cause a reduction of interface excursion. This is confirmed numerically (see next section).

Before closing this section we would like to discuss the validity of the amplitude theory in directional solidification. One special feature of this system lies in the flatness of the Mullins-Sekerka[16] spectrum. If time and length are measured in units of l^2/D and l, respectively, the curvature of the growth rate [Eq. (8)] yields close to criticality, and in the domain of interest ($\bar{q}\gg 1$)

$$-\frac{1}{2}\frac{\partial^2\bar{\omega}}{\partial\bar{q}^2}\simeq\frac{2(2k)^{1/3}\bar{d}_0^{2/3}}{1+\bar{b}_{\rm kin}(2k/\bar{d}_0)^{1/3}} .$$

Since, as mentioned before, $\bar{d}_0$ is small ($\bar{d}_0\sim 10^{-4}-10^{-3}$), $-\frac{1}{2}\partial^2\bar{\omega}/\partial\bar{q}^2$ is small compared to unity. In the absence of kinetics, for example, $-\frac{1}{2}\partial^2\bar{\omega}/\partial\bar{q}^2\sim 10^{-2}-10^{-1}$. This value is to be compared to that found in the Rayleigh-Bénard system,[19] which is of about 10. The flatness of $\bar{\omega}(\bar{q})$ implies that even if the actual velocity is close to the critical one, the dynamics of higher harmonics (essentially the second and third ones) are slow enough to efficiently contribute to the interface evolution. In other words, the band $\Delta\bar{q}$ of linearly active modes is wide enough. To be more precise, we expect the amplitude theory to accurately describe the interface dynamics when $\Delta\bar{q}/\bar{q}$ is small in comparison to unity. Using Eq. (12) together with Eq. (12) we obtain ($\bar{b}_{\rm kin}\equiv 0$ and $\bar{q}_c\gg 1$)

$$\left[\frac{\Delta\bar{q}}{\bar{q}}\right]^2\simeq k^{-2/3}\bar{d}_0^{-1/3}\left[\frac{v-v_c}{v_c}\right]$$

where we have set $\bar{l}_T=\frac{1}{2}$ (which corresponds to the threshold). For the ratio $\Delta\bar{q}/\bar{q}$ to be small the reduced value of the distance from threshold, $(v-v_c)/v_c$, should satisfy

$$\frac{v-v_c}{v_c}\ll k^{2/3}\bar{d}_0^{1/3} .$$

Since $\bar{d}_0\ll 1$, the range of validity of the amplitude theory is drastically restricted. For example, if $k=1$ and $\bar{d}_0=10^{-3}$ (which is a typical value) we get

$$\frac{v-v_c}{v_c}\ll 10^{-1} .$$

We should mention that the range of validity is even smaller in the presence of kinetics. Note also that the fact that the amplitude theory applies in an extremely narrow interval was demonstrated before in the study of phase dynamics.[20]

VI. THE FULLY NONLINEAR REGIME

To deal with the fully nonlinear regime we adapt the numerical code, developed previously,[10] to the present situation. This numerical method is the extension of the version first developed for the free dendrite problem.[21] We shall repeat here the main lines and emphasize the difference with the kinetics-free problem. The first step consists in converting the basic equations (1)–(3) into an integral equation which relates the concentration field u to its normal derivative $\partial u/\partial n$ at the liquid-solid interface. This can be accomplished by means of Green's-function techniques. The result is[21]

$$\int d\Gamma' g(\mathbf{r},\mathbf{r}')\frac{\partial u}{\partial n'}=\int d\Gamma' h(\mathbf{r},\mathbf{r}')u(\mathbf{r}') , \tag{49}$$

where the integration is performed along the liquid-solid boundary and where $g(\mathbf{r},\mathbf{r}')$ is the Green's function

$$g(\mathbf{r},\mathbf{r}')=\frac{1}{2\pi}e^{-(z-z')/l}K_0(\|\mathbf{r}-\mathbf{r}'\|/l) \tag{50a}$$

and

$$h(\mathbf{r},\mathbf{r}')=\frac{\partial g}{\partial n}-2l^{-1}n_z'g-c(\mathbf{r}')\delta(\mathbf{r}-\mathbf{r}') , \tag{50b}$$

where K_0 is the modified Bessel function. Expression (50a) represents the stationary propagator associated with the stationary version of Eq. (1). This is the so-called quasistationary limit, which is justified as long as the interface motion is slow as compared to the relaxation of the diffusion field. Finally the coefficient $c(\mathbf{r}')$ that enters Eq. (50b) originates, as explained previously,[21] from the fact that the volume integral $\int d\mathbf{r}'$ of the δ function is not unity since $\mathbf{r}'$ lies on the boundary Γ. If, for example, the boundary curve has a corner at $\mathbf{r}'$ with an angle $\phi(\mathbf{r}')$, then $c(\mathbf{r}')=\phi(\mathbf{r}')2\pi$. We shall see below that $c(\mathbf{r}')$ does not, in fact, need to be evaluated explicitly. As will be shown later this is because we shall make use of a global property of h:

$$\int d\Gamma' h(\mathbf{r},\mathbf{r}')=-1 . \tag{51}$$

This is a sum rule which expresses a general property of Green's functions.[21]

For $k=1$ (constant miscibility gap), and after making use of Eqs. (2) and (3), Eq. (4) can be written as

$$\int d\Gamma' \tilde{g}(\mathbf{r},\mathbf{r}')\frac{\partial u}{\partial n'}=\int d\Gamma' h(\mathbf{r},\mathbf{r}')\tilde{u}(\mathbf{r}') , \tag{52}$$

where

$$\tilde{g}(\mathbf{r},\mathbf{r}')=g(\mathbf{r},\mathbf{r}')-B_{\rm kin}h(\mathbf{r},\mathbf{r}') , \tag{53a}$$

$$\tilde{u}=1-d_0\kappa-\frac{\zeta}{l_T}+B_{\rm kin}v . \tag{53b}$$

We are now in a position to describe the strategy of the numerics. For a given pulling speed v and external thermal gradient we fix an initial morphology of the liquid-solid interace, $\zeta_0(x,t)$, at time t. For this interface configuration g, h, and $\tilde{u}$ can be calculated. Then by using Eq. (52) the normal gradient $\partial u/\partial n'$ at the interace will be obtained. This operation includes essentially an inversion of the matrix associated with the kernel $\tilde{g}$. From the continuity equation (2) the normal velocity v_n will be determined. In order to obtain the new interface configuration at time $t+\delta t$ each point on the previous position $\zeta_0(x,t)$ will be displaced by the amount $v_n\delta t\mathbf{n}$ in normal direction. We then repeat the same procedure on the new configuration and so on until the interface reaches a permanent regime (if any).

We should mention that in contrast to the case without kinetics[10] the constant miscibility gap assumption greatly simplifies the numerical procedure since Eq. (52) is linear in $\partial u/\partial n$. Had we let k be arbitrary, Eq. (49), combined with Eqs. (2) and (3), would have yielded a nonlinear equation for $\partial u/\partial n$, which would have required an iterative scheme of Newton-Raphson type. We have chosen $k=1$ here to avoid this additional difficulty. Since in the absence of kinetics the value of the partition coefficient did not seem to significantly alter the main conclusions in the developed nonlinear regime, we continue to believe here that the constant miscibility gap model captures the essential features of pattern formation. We should, of course, keep in mind that, in the vicinity of the planar front transition, the value of k may be decisive regarding the nature of the bifurcation. We hope to extend our calculation to the general case in the near future.

We shall now deal with the numerical technique. Since the solidification front shows various periodic structures above the critical velocity, we shall assume that it takes a structure with a fixed primary spacing or wavelength λ. This means that we do not address the question of wavelength selection. Moreover, we assume axisymmetric growth. This allows us to restrict our integration to a half period only. Equation (52) can then be written as

$$\int_0^{\lambda/2}d\Gamma'\sum_{m=-\infty}^{\infty}[\tilde{g}(x,\zeta|x'+m\lambda,\zeta')+\tilde{g}(x,\zeta|-x'+m\lambda,\zeta')]\frac{\partial u}{\partial n'}$$
$$=\int_0^{\lambda/2}d\Gamma'\sum_{m=-\infty}^{\infty}[h(x,\zeta|x'+m\lambda,\zeta')+h(x,\zeta|-x'+m\lambda,\zeta')+]\tilde{u} . \tag{54}$$

In standard experiments the Péclet number $P=\lambda/l$ is of the order of unity. Since the Green's function g as well as h decay exponentially fast, summation over $|m|\le 5$ periods is sufficient for most numerical simulations. To solve the one-dimensional integral equation (54) we use, as in the free dendrite problem,[21] the boundary element method. The boundary curve is discretized into a polygon symmetric to the z axis, whose corner points $\{\mathbf{r}_j;j=-N,\ldots,0,1,\ldots N\}$ (N is the number of grid points) satisfy the relation $x_{-j}=-x_j$ and $\zeta_{-j}=\zeta_j$. The function $\tilde{u}$ and the normal derivative of the diffusion field $w=\partial u/\partial n$ at a corner point $\mathbf{r}_j$ are symmetric; $\tilde{u}_{-j}=\tilde{u}_j$, $w_{-j}=w_j$. A point $\mathbf{r}$ on the polygon edge between the corners $\mathbf{r}_j$ and $\mathbf{r}_{j+1}$ is parameterized by a parameter ξ between -1 and $+1$ as

$$\mathbf{r}=\Phi_1(\xi)\mathbf{r}_j+\Phi_2(\xi)\mathbf{r}_{j+1}=\mathbf{r}_j+\Phi_2(\xi)\mathbf{s}_j , \tag{55}$$

where

$$\Phi_1(\xi)=\frac{1-\xi}{2},\quad \Phi_1(\xi)=\frac{1+\xi}{2} , \tag{56}$$

and

$$\mathbf{s}_j=\mathbf{r}_{j+1}-\mathbf{r}_j,\quad s_j=\|\mathbf{s}_j\| \ . \tag{57}$$

The integration along the segment $(\mathbf{r}_j,\mathbf{r}_{j+1})$ is written as

$$\int_{\mathbf{r}_j}^{\mathbf{r}_{j+1}}=\frac{s_j}{2}\int_{-1}^{+1}d\xi \ . \tag{58}$$

The curvature of $\mathbf{r}_j$ is determined as the inverse of the radius of the circle which passes three consecutive points $\mathbf{r}_{j-1},\mathbf{r}_j,\mathbf{r}_{j+1}$, and the normal $\mathbf{n}$ is a unit vector pointing from the center of the circle to the point $\mathbf{r}_j$. To complete the discretization scheme, the functions $\tilde{u}$ and w are approximated on each boundary element by the linear interpolation of their values at the end points $\mathbf{r}_j$ and $\mathbf{r}_{j+1}$ as

$$\tilde{u}(\xi)=\Phi_1(\xi)\tilde{u}_j+\Phi_2(\xi)\tilde{u}_{j+1} \ , \tag{59}$$

$$w(\xi)=\Phi_1(\xi)w_j+\Phi_2(\xi)w_{j+1} \ . \tag{60}$$

The integral equation (54) can then be written as a matrix equation

$$\sum_{j=-N}^{N}\tilde{G}_{ij}w_j=\sum_{j=-N}^{N}H_{ij}\tilde{u}_j \ , \tag{61}$$

where

$$H_{ij}=\frac{s_j}{2}\sum_m\int d\xi\, h(x_i,\zeta_i|x_j\Phi_1(\xi)+x_{j+1}\Phi_2(\xi)+m\lambda,\zeta_j\Phi_1(\xi)+\zeta_{j+1}\Phi_2(\xi)\Phi_1(\xi))$$
$$+\frac{s_{j+1}}{2}\sum_m\int d\xi\, h(x_i,\zeta_i|-x_j\Phi_1(\xi)-x_{j+1}\Phi_2(\xi)+m\lambda,\zeta_j\Phi_1(\xi)+\zeta_{j+1}\Phi_2(\xi)\Phi_2(\xi)) \tag{62a}$$

and

$$\tilde{G}_{ij}=H_{ij}(h\to g)-B_{\rm kin}H_{ij} \ . \tag{62b}$$

Integrals in Eqs. (62a) and (62b) are performed by a four point Gaussian integration. At the end points of the integrals, the logarithmic singularity[22] of the Green's function g needs a special treatment. Close to an end point where $\|\mathbf{r}-\mathbf{r}'\|$ becomes small

$$g\sim e^{-(\zeta-\zeta')}[-\ln(\|\mathbf{r}-\mathbf{r}'\|/2l)-\gamma] \ , \tag{63}$$

where γ is the Euler constant $\gamma=0.5772\ldots$. To evaluate the resulting integrals we make use of Gaussian integration for integrands with a logarithmic singularity.[22]

Finally the sum rule (50) reads, in the discretized version,

$$\sum_{j=-N}^{N}H_{ij}=-1 \tag{64}$$

from which the diagonal element H_{ii} is determined as

$$H_{ii}=-\sum_{j(\neq i)}H_{ij}-1 \ . \tag{65}$$

Since the coefficient $c(\mathbf{r}')$ entering expression (49a) will contribute only to the diagonal elements of the matrix H, it need not be evaluated explicitly, since it is absorbed in the H_{ii} determined from the sum rule.

The linear equation (61) is solved to give the gradient $w_j=\partial u_j/\partial n_j$ at a corner $\mathbf{r}_j$, which then determines the local normal velocity $u_{n,j}$ through Eq. (2) (recall that $k=1$). Then each point $\mathbf{r}_j$ moves by the amount $-Dw_jn_j\delta t$ in a short interval time δt. The time increment is chosen small enough to avoid numerical instabilities. As the distance between two neighboring points on the interface changes after each time iteration, the grid spacings s_j are dynamically adjusted at each time step to fall in an interval

$$s_{\max}/2<s_j<s_{\max}$$

which means that a corner is added on the polygon (in the middle of an averaged arc between $\mathbf{r}_j$ and $\mathbf{r}_{j+1}$) or eliminated according to whether s_j exceeds $s_{\max}$ or is smaller than $s_{\max}/2$.

To be definite, the material parameters for steel with Cr-Ni ingredients[23] are used. This allows us to make comparisons with previous results.[10] The units hereafter are chosen so that the thermal length l_T and diffusion constant D are equal to unity. In these units the capillary length $d_0=2.9510^{-4}$. The partition coefficient $k\simeq 1$. The critical velocity and wavelength computed from Eq. (11) are $v_c=1.14$ and $\lambda_c=0.5$. First of all we deal with the linear and weakly nonlinear regimes. Starting from an initial sinusoidal perturbation we have found that, within 1% uncertainty, the interface develops a cellular structure or rather decays into a planar form according to whether v is below or above the Mullins-Sekerka[16] threshold defined by Eq. (11).

Figure 2 shows a typical morphology of the solidification front slightly above threshold $[(v-v_c)/v_c\simeq 5\%,\ \lambda=\lambda_c]$ for $b_{\rm kin}=0.1$. Two remarks are in order. (i) The interface structure shows a strong deviation from a sinusoidal morphology, even close to

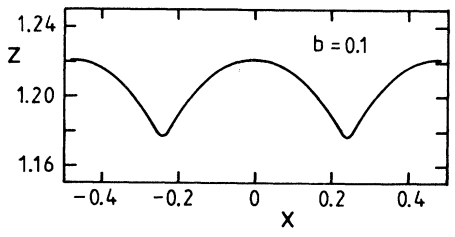

FIG. 2. A typical interface morphology close to the threshold $[(v-v_c)/v_c\simeq$ a few percent].

threshold. (ii) The departure from a sinusoidal form is more pronounced than in the absence of kinetics. This means, as predicted from the analysis of the dispersion relation (see last section), that kinetics reinforces the activation of higher harmonics. Shown in Fig. 3 are the Fourier amplitudes for $b_{\rm kin}=0.1$, compared to those obtained for $b_{\rm kin}=0$. In both cases one observes that higher harmonics are excited. For the kinetics-free case the amplitude of the second harmonic, for example, is about 15% that of the fundamental harmonic ($n=1$), while in the presence of kinetics it is 25%. On the other hand, the amplitude of the fundamental harmonic for $b_{\rm kin}=0$ is larger than the corresponding one when $b_{\rm kin}=0.1$. This result agrees with our expectations based on the amplitude theory, presented in the last section, which indicated that kinetics should reduce interface excursions.

Experiments tell us that when v increases the interface deformation becomes more and more pronounced, and on further increase of v, it evolves into a dendritic regime. Recently,[10] we dealt with the problem of dendritic growth without interface kinetics. We found that crystalline anisotropy is necessary to stabilize the tip of dendrite against splitting modes, exactly as found for the free-growth situation. The axial anisotropy due to the applied thermal gradient is not sufficient–at least in the range of parameters explored so far—to stabilize the tip. Moreover the scaling law for the tip radius follows the one found in the free-growth problem. The emission of side branches is apparent as soon as the Péclet number $P=\lambda/l=\lambda V/2D$ approaches unity. In the presence of kinetics, it is legitimate to think of pattern selection occurring on the basis of anisotropy of the kinetic coefficient. This plausibility was discussed by Brener and Mel'nikov[15] in the free-growth situation. It emerged from that analysis that for fourfold symmetry the growth velocity has the form

$$v=\left[\frac{2Db_{\rm kin}}{d_0}\right]^{9/2}\frac{\tilde{P}^{11/2}\alpha_{4\,\rm kin}^{7/2}}{\gamma_1 b_{\rm kin}} \tag{66}$$

with a constant prefactor $\gamma_1\simeq 0.2$, and where

$$\tilde{P}=vR/2D \tag{67}$$

with R the tip radius of dendrite.

To test the selection due to kinetics anisotropy, we have made a systematic calculation in dendritic regime. The anisotropy factor $\alpha_{4\,\rm kin}$ is taken to be equal to 0.1. If surface tension is isotropic, we find that anisotropic kinetics are sufficient to stabilize the pattern. Figure 4

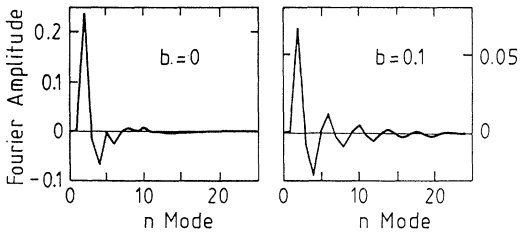

FIG. 3. The Fourier amplitudes close to the threshold.

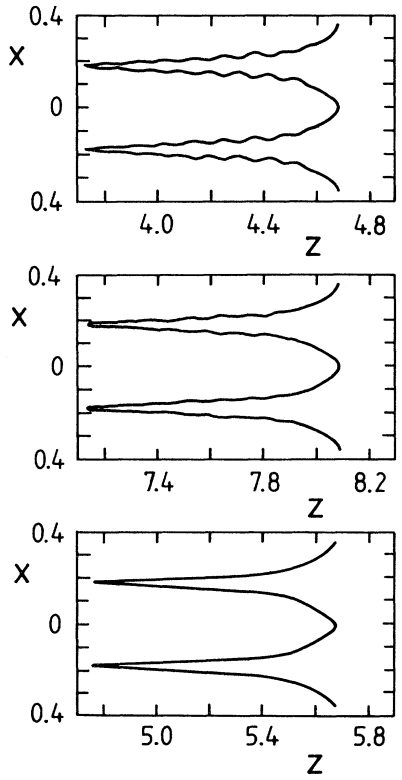

FIG. 4. The interface structure at $v=20$. Top: No kinetics (Ref. 10). Middle and bottom: Isotropic surface tension and $b_{\rm kin}=10^{-3}$ and 10^{-2}, respectively.

shows the pattern obtained at $v=20$ (recall that $v_c=1.14$) and $\lambda=0.36$ (as in our previous simulation[10]). Figure 4(a) corresponds to the kinetics-free case with anisotropic surface tension. Figures 4(b) and 4(c) correspond to $b_{\rm kin}=10^{-3}$ and 10^{-2}, respectively. There the surface tension is isotropic, while allowance is made for anisotropic kinetics. For higher values of $b_{\rm kin}$ the tip of dendrite becomes more and more angular, thus requiring higher numerical resolutions, which thereby considerably increases the computing time. Two remarks are in order. (i) The overall shape of dendrites selected by kinetic anisotropy is significantly different from that selected by surface-tension anisotropy [Fig. 4(a)]. The tip of the dendrite still remains parabolic, but slightly behind it the front develops quasiplanar sections [Fig. 4(c)]. (ii) The Péclet number for the present set of parameters is $P=3.6$, but even so the sidebranch activity is not efficient [or nonexistent in Fig. 4(c)]. This is to be contrasted with the selection based on surface-tension anisotropy [Fig. 4(a)]. In a WKB picture, where perturbations on the interface have a much smaller scale than the diffusion length, the interface can be considered as locally planar. Therefore the dispersion relation (40) for regression of fluctuations holds locally with $v\rightarrow v\cos(\theta)$, θ being the angle between the growth axis and the normal to the interface. We have seen in the preceding section that kinetics reduce interface excursions around a planar front. This means here that it should diminish the linear

development of side branches as $b_{\rm kin}$ increases. A more accurate treatment consists of specifying the basic state (a modified Ivanstov parabola including far sections) and studying the evolution of fluctuations on that state by writing down the evolution equation in real space, inspired by the dispersion relation (40). This is, however, beyond the scope of the present paper.

The interface morphology shown in Fig. 4(c) is very similar to that obtained[13] on impure CBr_4 (with P of a few unities). That shape appreciably differs from that obtained on *succinonitrile,* with an overall shape close to that displayed in Fig 4(a). It is tempting to conjecture that dendrites observed in this material are selected by kinetics anisotropy rather than by surface-tension anisotropy. Of course in reality both anisotropies are present. A natural question thus arises: If both anisotropies are competing, what would the final state be? More precisely will that state be essentially determined by one or other anisotropy or rather would we have a compromise between the two underlying mechanisms? An answer to this question is not at present available. It is nevertheless appealing to speculate that the generic situation would likely be the following. If the kinetic coefficient is not too large, the transition from cells to dendrites should be controlled by surface-tension anisotropy. As the growth velocity increases surface kinetics becomes of great importance and should become decisive. We then expect a transition to the selection on the basis of kinetic anisotropy. Whether such a transition occurs at reasonable values of the growth velocity depends on the importance of kinetics. It may even be possible that the first transition to dendrites is dominated by kinetics. This seems to be the case for CBr_4.

As mentioned above, a value of $\bar{b}_{\rm kin}$ which is appreciably bigger than 10^{-2} induces much sharper dendritic tips than those observed on impure CBr_4. This result leads one to expect that the kinetic coefficient in that system is not much larger than $\bar{b}_{\rm kin}\sim 10^{-2}$. Since $\bar{b}_{\rm kin}=vb_{\rm kin}$ and dendrites appear for $v\geq 10$, the value of the physical kinetic coefficient is at most $b_{\rm kin}\sim 10^{-2}$. Note that a typical thermal length is $l_T=100$ μm. This entails that the planar front recession due to kinetics is $\Delta\zeta=vb_{\rm kin}l_T\sim 1$ μm, when $v=1$ μm/s (a value for which the planar front is stable). This recession is small to be directly detected. For a thermal gradient $G\sim 100$ K, the front recession corresponds to a temperature shift $\Delta T\sim 10^{-2}$ K. An experimental access to such a small difference requires a sophisticated interface temperature measurement.

Finally to test the scaling law (66) obtained in the free-growth situation,[15] we have carried out calculations for different growth speeds. Figure 5 shows the results. There we compare the actual tip radius R with the radius $R_{\rm theor}$ obtained from the scaling relation (66), and alternatively with the Ivantsov radius $R_{\rm Iv}=\tilde{P}l$, where $\tilde{P}$ is taken as a measure of the supersaturation,

$$u(\text{tip})=\Delta=\sqrt{\pi\tilde{P}}\,e^{\tilde{P}}\,\text{erfc}(\sqrt{\tilde{P}}\,)\,, \tag{68}$$

where Δ is here the measured tip undercooling.

We can state that the scaling relation holds approxi-

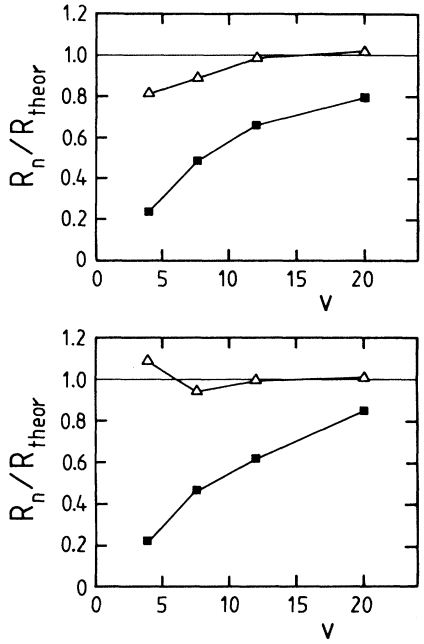

FIG. 5. Triangles: The ratio of actual tip radius to that obtained from calculations in the free-growth [Eq. (66)] case (Ref. 15) as a function of the pulling speed. Squares: The ratio of the Ivantsov tip radius to the one obtained from Eq. (66). The kinetic coefficient is $b_{\rm kin}=0.1$.

mately down to velocities as low as $v\simeq 4$ where the cells do not exhibit parabolic tips. At lower velocities the interface undercooling should approach the value $1+b_{\rm kin}v$ for a planar front. The fact that the scaling law (66) also holds for small velocities is consistent with the idea according to which the selection process is dominated by the behavior near the tip of the dendrite. The Ivantsov relation, however, does not hold for small velocities. This is not surprising as we know that this relation represents basically a global conservation law for an isolated parabolic cell.

In summary, we have analyzed interface structures in the presence of noninstantaneous interface kinetics. We have performed the linear stability analysis of the planar front solution. We found that the effect of kinetics is perturbative only if the kinetic coefficient is much smaller than unity. With the help of a third-order expansion we have shown that the nature of the bifurcation in the constant miscibility gap is unaffected by kinetics. Our analysis in the weakly nonlinear regime has allowed us to expect that higher harmonics should be excited by kinetics and that kinetics reduce interface excursions about the planar front. These expectations were confirmed by numerically integrating the original growth equations. The numerical method used here is the extension of the version used in free dendritic growth.[21] It consists of a forward time-dependent calculation, with a boundary element discretization scheme. In particular, this method allows us to study the dendritic regime. The interface structure is found to exhibit an "angular" feature, in contrast to the smooth structure based on selection by

surface-tension anisotropy.[10] Another striking feature found here is that side-branch activity is weak. The fact that dendrites observed on impure CBr_4 (Refs. 13 and 14) exhibit similar features has led us to postulate that dendrites in that system are selected by kinetic anisotropy. The scaling law for the selection of tip radius[15] by kinetics anisotropy was recovered at values of the speed such that the diffusion length becomes comparable to the primary spacing. The same result was found when selection is based on surface energy anisotropy.[10]

One important question which remains open concerns the competition of the two selection mechanisms (related to surface-tension and kinetics anisotropies). An interesting case is the one when the directions of the minima of the surface-tension and kinetic coefficient anisotropies do not coincide.

ACKNOWLEDGMENTS

We are grateful to S. de Cheveigné for a critical reading of the manuscript.

APPENDIX

We list here the various amplitudes that enter the second-order contribution to the interface position and concentration field. All these quantities are understood to be evaluated at the bifurcation. The coefficients β_{20} and ζ_{20} that multiply $\|A\|^2$ in Eqs. (25a) and (25b) are

$$\beta_{20}=\frac{1}{l^2}-\frac{m_c k/l}{l m_c/2-1+k}-b_{\rm kin}v_c q_c^2\frac{l_T}{2l}\ ,$$

$$\zeta_{20}=\tfrac{1}{4}l_T b_{\rm kin}v_c q_c^2\ .$$

The coefficient multiplying the second harmonic term in Eqs. (25a) and (25b) can be written as

$$\zeta_{22}=\frac{(v_c-Dm_c')\left[1/l^2-\dfrac{km_c/l}{m_c l/2-1+k}+b_{\rm kin}v_c q_c^2/4\right]-b_{\rm kin}kq_c^2v_c^2-\dfrac{kv_c q_c^2}{m_c l/2-1+k}}{2v_c k/l+[v_c(1-k)-Dm_c'](-4q_c^2d_0+2/l-1/l_T)}$$

and β_{22} is related to ζ_{22} by

$$\beta_{22}=(2/l-1/l_T)\zeta_{22}-4q_c^2d_0\zeta_{22}-1/l^2-\frac{m_c k/l}{m_c l/2-1+k}+b_{\rm kin}v_c q_c^2/4\ .$$

The Landau constant that enters the amplitude equation [Eq. (35)] reads

$$\omega_1=\left[1/v_c+b_{\rm kin}M-\frac{k}{(m_c l-1)Mv_c}\right]^{-1}l^3/v\left[4(m_c l/2-1)\zeta_{20}/l^2+\zeta_{22}\left[\frac{2(m_c l/2-1)}{l^2}-\frac{q_c^2k}{M}-b_{\rm kin}Mv_c q_c^2\right]\right.$$
$$+2\beta_{20}(1-m_c l/2)/l+\tfrac{1}{2}\beta_{22}l[m_c'(m_c'-m_c)/2-q_c^2]$$
$$\left.+\frac{1}{l^3}(1-m_c l/2)-\tfrac{3}{8}Mq_c^2d_0+\frac{km_c q_c^2}{4M}\right]$$

with $M=m_c l/2+k-1$.

Finally the α coefficient that enters the third-order contribution [Eq. (30)] has the form

$$\alpha=\frac{1}{vM}\left[b_{\rm kin}vM+1+\frac{k}{(2m-1)M}\right]\ .$$

*Permanent address: Groupe de Physique des Solides, associé au Centre National de la Recherche Scientifique, 2 Place Jussieu, 75005 Paris, France.

†Permanent address: Physics Department, Keio University, Yokohama, Japan.

[1]For a recent review, see H. Müller-Krumbhaar and W. Kurz (unpublished).

[2]D. J. Wollkind and L. A. Segel, Philos. Trans. R. Soc. London **51**, 268 (1970).

[3]J. S. Langer and L. A. Turski, Acta Metall. **24**, 1113 (1977).

[4]J. S. Langer, Acta Metall. **25**, 1121 (1977).

[5]B. Caroli, C. Caroli, and B. Roulet, J. Phys. **43**, 1767 (1982).

[6]G. Dee and R. Mathur, Phys. Rev. B **27**, 7073 (1983).

[7]L. H. Ungar and R. A. Brown, Phys. Rev. B **29**, 1367 (1984); **30**, 3993 (1984); **31**, 5923 (1985); **31**, 5931 (1985).

[8]N. Ramprassad, M. J. Benett, and R. A. Brown, Phys. Rev. B **38** 583 (1988).

[9]D. Kessler and H. Levine, Phys. Rev. A **39**, 3041 (1989).

[10]Y. Saito, C. Misbah, and H. Müller-Krumbhaar, Phys. Rev. Lett. **63**, 2377 (1989).

[11]C. Misbah, H. Müller-Krumbhaar, and Y. Saito, J. Cryst. Growth **99**, 156 (1990).

[12]H. Esaka and W. Kurz, J. Cryst. Growth **72**, 578 (1985).
[13]P. Kurowski, thèse, Université de Paris 7, 1990.
[14]P. Kurowski, C. Guthmann, and S. de Cheveigné (unpublished).
[15]E. A. Brener and V. I. Mel'nikov (unpublished).
[16]W. W. Mullins and R. F. Sekerka, J. Appl. Phys. **35**, 444 (1964).
[17]A. C. Newell and J. A. Whitehead, J. Fluid. Mech. **38**, 279 (1969).
[18]L. A. Segel, J. Fluid. Mech. **38**, 203 (1969).
[19]P. G. Drazin and W. H. Reid, *Hydrodynamic Stability* (Cambridge University Press, Cambridge, England, 1981), p. 50.
[20]K. Brattkus and C. Misbah, Phys. Rev. Lett. **64**, 1935 (1990).
[21]Y. Saito, G. Goldbeck-Wood, and H. Müller-Krumbhaar, Phys. Rev. A **38**, 2148 (1988).
[22]*Handbook of Mathematical Functions,* edited by M. Abramowitz and I. A. Stegun (Dover, New York, 1972), p. 875.
[23]G. Lesoult (private communication).